

Timescale Monitoring of Vesuvian Eruptions Using Numerical Modeling of the Diffusion Equation

Julien Amalberti^{1,3} · Xavier Antoine² · Pete Burnard¹

Received: 28 July 2017 / Accepted: 13 February 2018 / Published online: 26 March 2018
© International Association for Mathematical Geosciences 2018

Abstract It is necessary to understand the diffusive behavior of the volatile phase in order to interpret the control mechanisms of the bubble size in volcanic rocks and the processes influencing the eruption itself. A simple numerical model is proposed, based on the time-dependency of the diffusion equation for a hollow sphere, to simulate incorporation of atmospheric noble gases in pumice for Vesuvian (i.e., Plinian) eruptions. During a Vesuvian eruption, melt fragments are ejected into the air. The resulting pumice samples collected after the eruption phase exhibit a significant incorporation of elementally and isotopically fractionated atmospheric noble gases. The noble gas content of the trapped gases then potentially provides useful data with which to constrain the timescales of cooling for the samples. The system can be adequately described as a diffusion process into a hollow sphere through the one dimensional diffusion equation for a spherically symmetrical geometry. Diffusion coefficients are time-dependent to include the effect of an exponential decay of temperature with time. The complexity of this system requires numerical resolution of the diffusion equation due to the diffusion coefficient temperature dependency. The outer boundary condition is fixed with a given noble gas concentration via an inhomogeneous Dirichlet boundary condition, while the inner boundary condition is set as a flux-free boundary.

Dedicated to the memory of Pete Burnard who passed away in July 2015.

✉ Julien Amalberti
jvamalbe@umich.edu

¹ Centre de Recherche Péetrographique et Géochemique, 15 Rue Notre-Dame des Pauvres, B.P. 20, 54001 Vandoeuvre Cedex, France

² Institut Elie Cartan de Lorraine, Université de Lorraine, Inria Nancy-Grand Est, 54506 Vandoeuvre-lès-Nancy Cedex, France

³ Present Address: Department of Earth and Environmental Sciences, University of Michigan, Ann Arbor, MI, USA

The numerical model allows the noble gas content, and thus the noble gas elemental and isotopic ratios entering the bubble, to be modeled as a function of time, hollow sphere thickness, diffusion coefficients, initial and final temperatures, and quench rate.

Keywords Diffusion processes · Vesuvian eruption · Noble gas · Numerical modeling

1 Introduction

Numerical approaches of kinetic processes during magma degassing have important applications in the study of nucleation and bubble growth. Nucleation and bubble growth are important processes for understanding eruption mechanisms and degassing processes (Sparks et al. 1978). Nucleation is controlled by growth through the depletion of the degassing component from melt. For example, Toramaru (1995) numerically solved nucleation and growth processes of bubbles in viscous melts based on a formulation involving viscosity effects on nucleation and moments of bubble size distribution. Proussevitch and Sahagian (2005) also investigated the dynamics of diffusive bubble growth in magmas. Their numerical model includes the effect of gas diffusion in the melt, the hydrodynamics of the melt surrounding growing bubbles and the complex interaction between hydrodynamics and diffusion. The model is based on a cell model describing diffusion-induced growth of closely spaced bubbles in melts. Their numerical model reveals the sensitivity of the diffusive bubble growth related to the distances between two bubbles within the magma, the volatile concentration in the melt, the initial pressure, the viscosity of the liquid, and the diffusivity of the gas. Such documentation of the evolution of gas fraction in the melt and bubble wall thickness as a function of time makes it possible to estimate bubble disruption thresholds, which bear on volcanic eruption mechanisms. Model results can be applied to the larger-scale problem of magmatic degassing in terms of bubble coalescence, flotation and the development of foams in magma chambers, vent systems and ultimately to the dynamics of eruption mechanisms (Proussevitch and Sahagian 2005). Proussevitch and Sahagian (2005) developed a numerical model characterized by treatment of the transient problem, specific eruption triggers (as instantaneous decompression events), disequilibrium degassing, full-scale bubble growth module and steady-state eruption. They found that the conduit geometry is critical to determining the nature of the eruption. They also observed that the eruption occurs within 2 min of the trigger, showing the rapidity of the degassing.

These studies have demonstrated that numerical modeling is a powerful tool for studying and improving our understanding of magma degassing processes. They show that the growth of bubbles and nucleation as a consequence of volatile exsolution has a major impact on the dynamism of the volcanic eruption. Bubble growth rates are controlled by volatile diffusion rates, eruption timescales and volatile solubility. Volcanic eruptions are usually thought to be driven by exsolution of a volatile phase under magmatic conditions such as elevated temperature and pressure (Anderson 1975; Sparks et al. 1978; Sparks 2003; Tait et al. 1989; Jaupart 2000). Non-equilibrium fractionation among volatile phases, driven by their different diffusivities, are known to be common during magma decompression and degassing (Paonita and Martelli 2007; Gonnermann

and Mukhopadhyay 2007). Recently, studies on both elemental and isotopic noble gas ratios have recorded non-equilibrium fractionation in pumice in which some vesicles are preserved (Pinti et al. 1999; Ruzié and Moreira 2010). Noble gases are known to be chemically inert, and thus can be used to investigate physical processes during magma degassing. Even if such fractionations are related to kinetic processes, they are rarely observed in terrestrial samples (Kaneoka 1980). Fractionation has been calculated by diffusion of noble gases in pumice vesicles through a glass wall (i.e., after pumice quenching) (Pinti et al. 1999). Pinti et al. (1999) concluded that noble gas isotopic and abundance fractionations (relative to the atmospheric composition) reflect the initial magmatic temperature, the cooling rate of the eruption column and the bubble's wall thickness. However, based on the Proussevitch and Sahagian (2005) cell model, Ruzié and Moreira (2010) determined that noble gas diffusion through the liquid shell (i.e., at magmatic temperature) can explain the observed noble gas fractionation in pumice without requiring a post-quenching diffusion. Their model was able to determine characteristic times of magma ascent on the order of a few 100 s. Ruzié and Moreira (2010) also demonstrated that Ar diffusion through the glass shell at ambient temperature would be too slow to generate the compositions observed and concluded, instead, that the fractionation processes must have occurred in the magmatic phase, prior to fragmentation. Both of the studies used either linearly decreasing (Pinti et al. 1999) or constant (Ruzié and Moreira 2010) temperature. However, Amalberti et al. (2016) showed that heavy noble gas diffusivities (e.g. Ar) recorded in silicate glass close to the T_g , the glass transition temperature, are sufficient to allow incorporation and kinetic fractionation of atmospheric noble gases on timescales that are reasonable for Plinian eruptions. Nevertheless, the temperature dependency of the diffusion equation during eruption has never been investigated through numerical modeling. A simple but rigorous numerical simulation is proposed to examine the potential incorporation of gases, notably noble gases, into a preexisting bubble during the cooling stages of magma (i.e., exponential decrease of the temperature). This numerical model provides new insights into the behavior of the volatile phase during the extreme temperature variations that take place during magma quenching. More generally, the numerical model presented here can be applied in studies where the variation of the diffusion equation as a function of temperature is needed.

2 Starting Equation and Approach Undertaken

Variations of diffusion coefficient related to the exponential decreasing of temperature have never, up to now, been applied to a degassing model that attempts to explain the signature of the volatile phase during magma degassing. Previous models used simple approximations of temperature behavior during eruptions that do not accurately reflect the time-dependent behavior of diffusivities. In order to investigate the incorporation and fractionation of atmospheric noble gases into the bubbles, hollow sphere geometry was used. Similarly to Pinti et al. (1999), the gases are allowed to diffuse through a hollow sphere, based on a specific mathematical solution of the diffusion equation given by Crank (1975)

$$\frac{M_t}{M_\infty} = 1 - \frac{6}{\pi^2 (a^2 + ab + b^2)} \sum_{n=1}^{\infty} \left(\left(\frac{b \cos(n\pi - a)}{n} \right)^2 e^{-\frac{Dn^2\pi^2 t}{(b-a)^2}} \right), \quad (1)$$

where M_t/M_∞ is the gas fraction entering or leaving the hollow sphere at the specific time t , a and b being the hollow sphere limits ($a \leq r \leq b$). However, this solution is valid for a constant diffusion coefficient: Eq. (1) cannot be applied to evolving temperatures (and therefore diffusivities) that will occur when pumices erupt.

To further investigate this problem, the temperature dependency of diffusion given by the Arrhenius relation need to be taken into account

$$D(T) = D_0 e^{\frac{E_a}{RT}}, \quad (2)$$

where D_0 is the pre-exponential term, corresponding to an imaginary diffusivity at $T = \infty$, E_a is the activation energy for diffusion, and R is the gas constant.

A partial differential equation (PDE) for diffusion into a sphere (i.e., a hollow sphere) is also given by Crank (1975), which takes into account the temperature dependency of diffusion $D(T)$

$$\frac{\partial u}{\partial t} = D(T) \frac{\partial^2 u}{\partial r^2}, \quad (3)$$

where $u = Cr$, C is the concentration of the diffusing substance, r is the hollow sphere thickness, and $D(T)$ is the diffusion coefficient in Eq. (3). The relation that links the temperature (T) and time (t), for an exponentially temperature decay, is given by

$$T(t) = (T_Q - T_L) e^{-\frac{vt}{T_Q}} + T_L, \quad (4)$$

where T_Q and T_L are the initial and final temperatures (K), respectively, and v is the exponential cooling rate (K s^{-1}). There is no simple analytical solution to Eq. (3) with an exponentially decaying temperature, since the PDE includes some variable coefficients. To be able to simulate a temperature dependency on the diffusion equation coefficient (D) (Eq. 3), the initial equation given by Crank (1975) was used for a constant coefficient D (Eq. 2)

$$\frac{\partial u}{\partial t} = D \frac{\partial^2 u}{\partial r^2}. \quad (5)$$

A numerical model was developed where the temperature dependency of $D(T)$ can then be integrated easily by computing it at each time step during the simulation calculation, the updated value of D being given by combining Eqs. (2), (4) and (5)

$$\frac{\partial u}{\partial t} = D(T(t)) \frac{\partial^2 u}{\partial x^2}, \quad (6)$$

where $u = Cr$, setting C is the concentration of diffusing substance and r is the radius of the system. The diffusion coefficient $D(T(t))$ is temperature-dependent, t is the time variable and x the spatial radial coordinate.

3 Mathematical Model and Numerical Approximation

3.1 Mathematical Modeling

Following Eq. (5), two boundary conditions need to be added to the time-dependent diffusion equation at the endpoints a and b , the external and internal system boundary, respectively, and an initial boundary condition $u(t = 0, r) = u_0(r)$ to obtain a well-posed initial boundary-value problem. On the external boundary $r = b$, the value of the field u is fixed at a given constant gas concentration C_0 , [i.e., $u(t, b) = C_b$]. This boundary condition is known as the inhomogeneous Dirichlet boundary condition in the mathematics literature. At the internal boundary $r = a$, a free-barrier boundary condition: $\partial_r u(t, a) = 0$ is considered. Fixing the value of the normal derivative trace at $r = a$ to zero is called a homogeneous Neumann boundary condition. As a consequence, the full model that is considered in this paper is the following initial boundary-value problem: find the solution u to the evolution system

$$\begin{cases} \frac{\partial u}{\partial t} = D(t) \frac{\partial^2 u}{\partial r^2}, & \text{for } t > 0, a < r < b. \\ \partial_r u(t, r = a) = 0, & \text{for } t > 0. \\ C(t, r = b) = C_b & \text{for } t > 0. \\ u(t = 0, r) = u_0(r), & \text{for } a < r < b. \end{cases} \tag{6}$$

It can be rigorously proven that under suitable smoothness conditions, there exists one and only one solution u to this problem. The system being well-posed, it is now ready for a numerical approximation to get a computed solution.

3.2 Numerical Scheme

For the interior numerical solution, a Crank–Nicolson finite difference scheme (Press et al. 2007) was used, which is second-order accurate in time and unconditionally stable. In addition, a second-order centered scheme was used to approximate the second-order spatial derivative operator (Press et al. 2007). In order to solve system Eq. (6) from $t = 0$ to a maximal time t_{\max} , the interval $(0; t_{\max})$ is uniformly discretized into N segments $(t_n; t_{n+1})$, where $t_n = n\Delta t$, for $n = 0, \dots, N - 1$ with $t_0 = 0, t_N = t_{\max}$ and $\Delta t = t_{\max}/N$. Let’s now introduce a uniform discretization of $(a; b)$ by using J segments $(r_j; r_{j+1}), j = 0, \dots, J - 1$, with $r_0 = a, r_J = b$ and $h = (b - a)/J$. Following this notation, $r_j = a + jh$. The numerical approximation of the PDE arising in system Eq. (6) can be written as follows

$$\frac{u_j^{n+1} - u_j^n}{\Delta t} = D^{n+1/2} \frac{(u_{j+1}^{n+1} - 2u_j^{n+1} + u_{j-1}^{n+1}) + (u_{j+1}^n - 2u_j^n + u_{j-1}^n)}{2h^2} = 0, \tag{7}$$

with $D^{n+1/2} = (D^n + D^{n+1})/2$, for $n = 0, \dots, N - 1$ and $j = 0, \dots, J - 1$. The approximation of $u(t_n, r_j)$ is denoted by u_n^j . At the endpoint $r_0 = a$ and for consistency, the second-order centered spatial approximation of the normal derivative is used

$$\frac{(u_{-1}^{n+1} + u_{-1}^n)}{4h} = 0 \Rightarrow u_{-1}^{n+1} + u_{-1}^n = 4hCb + (u_1^{n+1} + u_1^n),$$

where $r_{-1} = a - h$ is a ghost discretization point outside the physical computational domain. Rewriting Eq. (7) for $j = 0$ and using the equation above provides the updating equation for the numerical discrete model

$$\frac{1}{\Delta t} + \frac{D^{n+\frac{1}{2}}}{h^2} u_0^{n+1} - \frac{D^{n+\frac{1}{2}}}{h^2} u_1^{n+1} = \frac{1}{\Delta t} - \frac{D^{n+\frac{1}{2}}}{h^2} u_0^n - \frac{D^{n+\frac{1}{2}}}{h^2} u_1^n. \tag{8}$$

Now, at point $r_j = b$, one gets the discrete equation for the Crank–Nicolson scheme

$$\frac{(u_j^{n+1} + u_j^n)}{2} = C_b \Rightarrow u_j^{n+1} = 2C_b - u_j^n. \tag{9}$$

Considering Eq. (7) for $j = J - 1$, the linear relation is deduced as follows

$$-\frac{D^{n+\frac{1}{2}}}{2h^2} u_{J-2}^{n+1} + \left(\frac{1}{\Delta t} + \frac{D^{n+\frac{1}{2}}}{h^2} \right) u_{J-1}^{n+1} = \frac{D^{n+\frac{1}{2}}}{2h^2} u_{J-2}^n + \left(\frac{1}{\Delta t} - \frac{D^{n+\frac{1}{2}}}{h^2} \right) u_{J-1}^n + \frac{D^{n+\frac{1}{2}}}{h^2} C_b. \tag{10}$$

The real-valued vector fields can be expressed as $\mathbf{u}^n = (u_j^n)_{0 \leq j \leq J-1} \in \mathbb{R}^J$ and $\mathbf{b}^n = (b_j^n)_{0 \leq j \leq J-1} \in \mathbb{R}^J$ such that $b_{J-1}^n = h^{-2} D^{n+1/2} C_b$, and $b_j^n = 0$ for $j = 0, \dots, J - 2$. The $J \times J$ real-valued sparse positive definite matrix is defined as follows

$$\mathbb{A} := \frac{1}{2h^2} \begin{pmatrix} 2 & -2 & 0 & \dots & 0 & 0 & 0 \\ 0 & -1 & 2 & -1 & 0 & 0 & 0 \\ 0 & 0 & -1 & 2 & -1 & 0 & 0 \\ 0 & \dots & \dots & \dots & \dots & \dots & 0 \\ 0 & \dots & 0 & -1 & 2 & -1 & 0 \\ 0 & 0 & 0 & \dots & 0 & -1 & 2 \end{pmatrix}. \tag{11}$$

Then, Eqs. (7), (8) and (10) can be recast under the form of a linear system

$$\left(\frac{\mathbb{I}}{\Delta t} + D^{n+\frac{1}{2}} \mathbb{A} \right) \mathbf{u}^{n+1} = \left(\frac{\mathbb{I}}{\Delta t} - D^{n+\frac{1}{2}} \mathbb{A} \right) \mathbf{u}^n + \mathbf{b}^n, \tag{11}$$

where \mathbb{I} is the identity matrix of size $J \times J$. If an initial datum u_0 is given, then the initial vector is trivially defined by $\mathbf{u}^0 = (u_0(r_j^n))_{0 \leq j \leq J-1}$. The resulting scheme is globally second-order in both space and time, and unconditionally stable. Each time step of the algorithm requires the numerical solution to the n -dependent linear system of Eq. (11). This can be done efficiently and accurately thanks to an LU factorization (Press et al. 2007) based on the Thomas algorithm for a tridiagonal system (Press et al. 2007). Therefore, each time step requires only about J elementary operations. The memory storage is very low and on the order of J . In conclusion, this solution provides a fast, accurate and stable numerical method for solving Eq. (6) for any time-dependent concentration function D .

4 The Resulting Code and How to use it

The Matlab source code is provided. The source code has been written for Matlab version 2014b. Issues might be encountered for earlier versions. Based on the previous discretization scheme, the Matlab solver has been developed in three parts: the main part, named “Diffusion_main.m”, consists of a GUI interface which calls two functions: “function_gas1.m” and “function_gas2.m”. The code is given in the supplementary material. Run the Diffusion_main script to launch the GUI interface. The model parameters and the GUI interface are shown in Fig. 1. The resulting data are plotted in three dimensions (time, distance and concentration). Data can be exported to an Excel file, which is automatically named “ResultsFiles.xlsx” comprised of sheet 1: the Gas 1 data, sheet 2: Gas 2 data; sheet 3: the ratio of Gas 1/Gas 2; sheet 4: the simulation time, and sheet 5: the corresponding temperature. Note that all the data are written in the first row of each sheet.

5 Application Examples

5.1 Numerical Validation of the Computational Model

A comparison of the results given by the numerical simulation to different experimental and analytical data and solutions is provided. Given that the model is derived

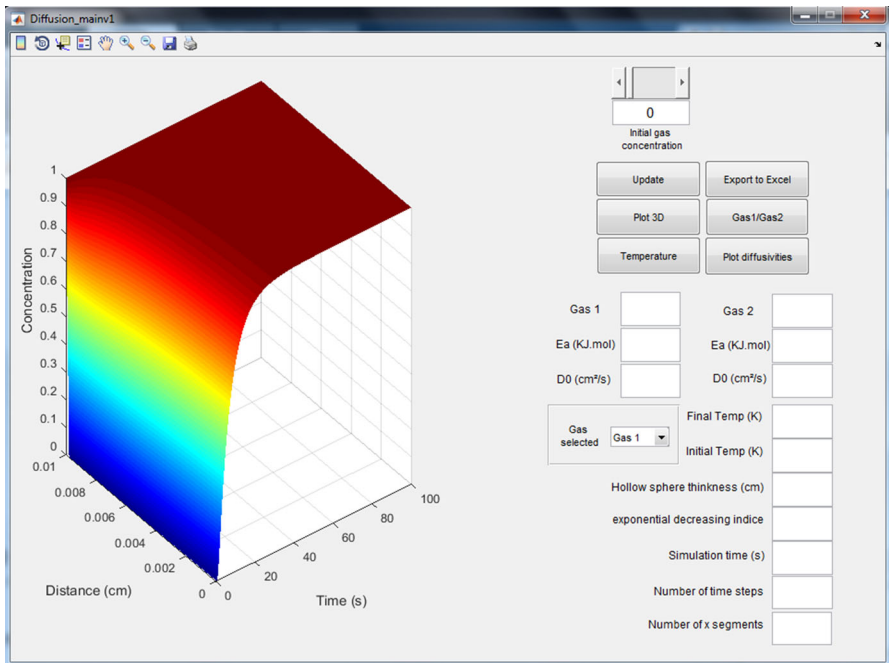


Fig. 1 Matlab GUI interface

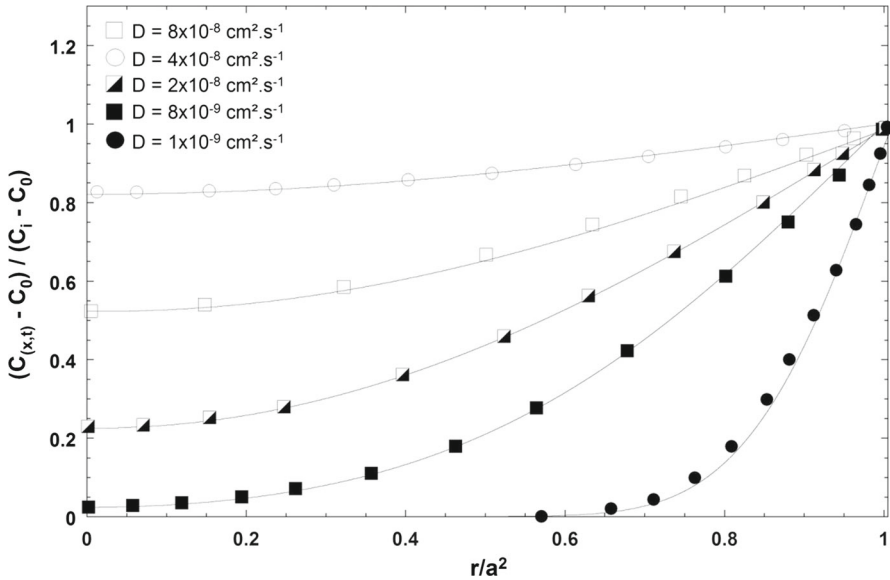


Fig. 2 Results of numerical (dark line) versus analytical (data points) solutions for the general diffusion Eq. (3) with constant D . Diffusion parameters are fixed with $t = 1000$ s (the simulation time) and $a = 0.01$ cm (the hollow sphere thickness). The x axis is expressed with the dimensionless parameter r/a^2 , with $r = 0$ and $r = a$, at respectively the center and the edges of the hollow sphere. Symbols are as follow: solid circle for $D = 1 \times 10^{-9} \text{ cm}^2 \text{ s}^{-1}$, solid square for $D = 8 \times 10^{-9} \text{ cm}^2 \text{ s}^{-1}$, half-filled square for $D = 2 \times 10^{-8} \text{ cm}^2 \text{ s}^{-1}$, open square for $D = 4 \times 10^{-8} \text{ cm}^2 \text{ s}^{-1}$ and open circle for $D = 8 \times 10^{-8} \text{ cm}^2 \text{ s}^{-1}$

from the general form of the diffusion equation for a constant D (Eq. 5) (Crank 1975), the output of the numerical solution for the D constant was compared with the analytical solution given by Crank (1975) for five different diffusion coefficients to validate the accuracy of the method. The results are shown in Fig. 2. A good agreement is observed between the analytical and the numerical solutions. Unfortunately, the analytical solution corresponding to our case is not provided by Crank (1975), even for a linear decay of the temperature. Dodson (1973) used time-dependent diffusion coefficients (i.e., a linear decrease of the temperature) in a problem of diffusion in a cooling solid in order to calculate the age of a rock or mineral from its accumulated products of radioactive decay. Although the diffusion equations are solved with an analytical solution, the addition of the radioactive decay brings a complexity not implemented in our numerical model. In addition, an important condition for validity of the theory in Dodson (1973) is that the cooling should be “slow”. Quantitatively, this means that τ , the time constant as defined by Dodson (1973), must be much greater than the characteristic diffusion time $a^2/D(0)$, where $D(0)$ is the diffusion coefficient at $t = 0$, and a is the characteristic dimension of the system. In this case, the cooling time constant is of the order of few 100 s for Ar diffusion in pumice during the quench. However, $a^2/D(0)$ is of the order of 10 min at a temperature of 1000 K. We consider an Ar diffusion coefficient at $1.3 \times 10^{-9} \text{ cm}^2 \text{ s}^{-1}$ at $T = 1100$ K (Amalberti et al., 2016) and a characteristic diffusion length of $10 \mu\text{m}$ for the pumice wall (Whitman

and Sparks 1986). Therefore, for the application (see below), the condition of a slow cooling rate is not satisfied as specified by Dodson (1973).

Next, the comparison was extended to the experimental databases for a thin-source diffusion experiment (Zhang and Cherniak 2010), for Th diffusion in a diopside melt at 1473 K (Van Orman et al. 1998) and for Ar diffusion in a rhyolitic melt (experiment RhyAr4-0) at 1375 K (Behrens and Zhang 2001). Thin source experiments mean that diffusion proceeds from the surface of the material into its interior. The thin-source experiments are performed at constant temperature (1473 K for Th and 1375 K for Ar) for a time of 70.65 h (Th) and 1800 s (Ar). Such experiments refer generally to the diffusion problem in a semi-infinite space, with the initial condition that all of the diffusing species are at a single location of $x = 0$; and $C = 0$ for $x > 0$. This mathematical problem is similar to that of a one-dimensional random walk where the gas diffusion is one-directional. Hence, the concentration profile (i.e., the solution to this diffusion problem) is given by (Crank 1975; Zhang and Cherniak 2010)

$$C(x, t) = \frac{M}{(\pi Dt)^{\frac{1}{2}}} e^{-\frac{x^2}{4Dt}} = C_0 e^{-\frac{x^2}{4Dt}}, \quad (12)$$

where x is the distance measured from the surface of the system, C_0 is the concentration at $x = 0$ and M is the initial mass of the diffusing atoms in the system per applied area. From Eq. (5), the constant diffusion D for Eq. (12) is derived. Thus, this problem corresponds to the presented model's description, with the sole exception that D is constant. Therefore, the numerical solution of Eq. (12) can be tested with the parameters given by the study authors, such as D (at a given T), the diffusion distance (x), and the experiment duration (t).

Results are displayed in Fig. 3 and show good reproducibility of the experimental data by the model. In addition, the model also predicts very well the concentration profile recorded by Carroll and Stolper (1991) (not shown here) for Ar diffusion in SiO₂ glass at a pressure of 200–3785 bars and temperatures of 673–1173 K.

5.2 Plinian Eruption Timescales

The ³⁸Ar/³⁶Ar isotopic and ⁸⁴Kr/³⁶Ar elementary ratios have been recently measured, in bubble bearing pumices, during the last Plinian eruption of Pelé Mountain in Martinique (Ruzié and Moreira 2010). This data base provides a study case for estimating the eruption timescale by using our numerical model, although Ruzié and Moreira (2010) argued that these kinetic fractionations may originate only under magmatic conditions (i.e., in the magmatic chamber). However, as pointed out by Pinti et al. (1999) and Amalberti et al. (2016), kinetic noble gas fractionation may occur during cooling of the magma. In order to document this possibility, a lava ejection from high temperature ($T_Q = 1,123$ K) to room temperature ($T_L = 298$ K) is simulated, using the diffusion coefficients from Matsuda et al. (1989) for ⁸⁴Kr in obsidian and Drapper and Carroll (1995) for Ar in Rhyolite, ³⁶Ar was calculated using Graham's law (Eq. 13)

$$\frac{D_A}{D_B} = \left(\frac{M_B}{M_A} \right)^\beta, \quad (13)$$

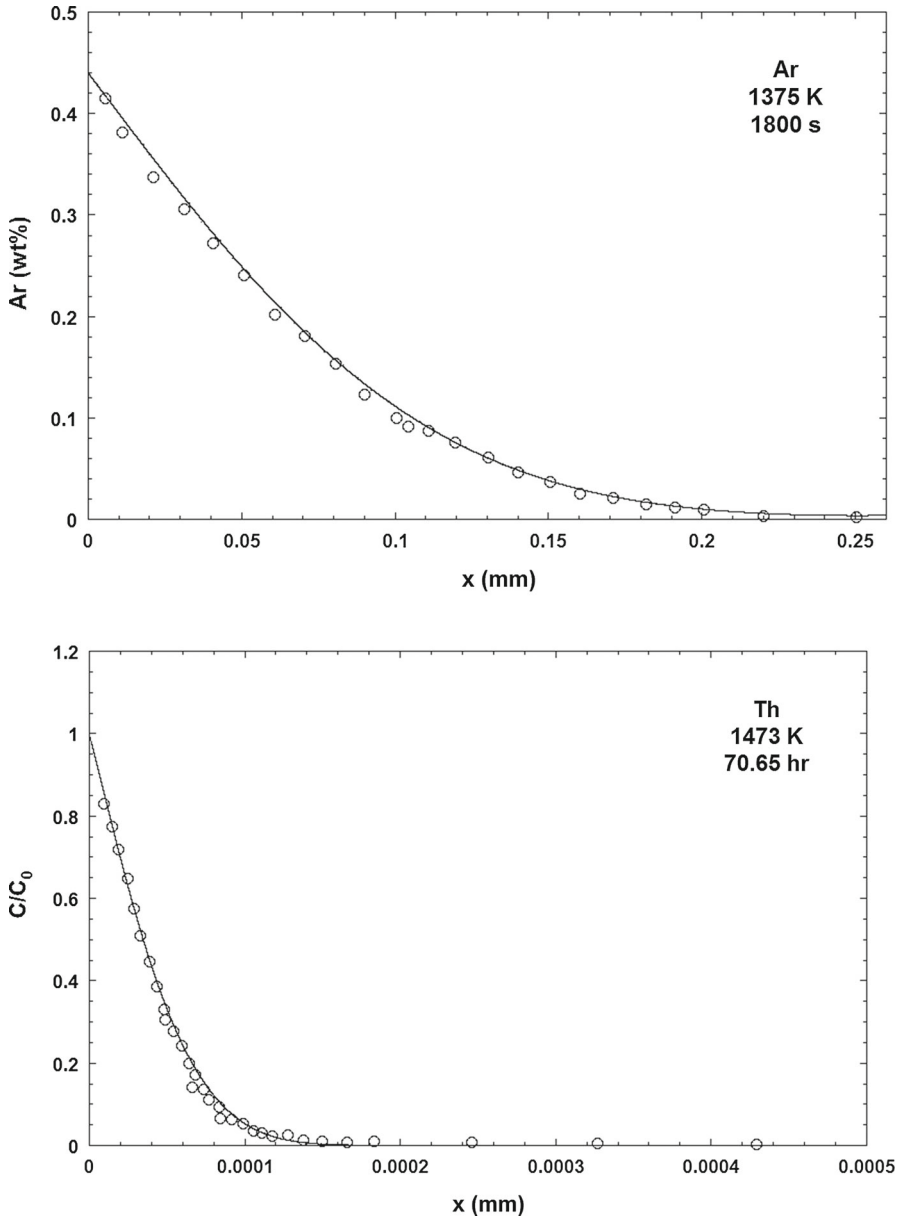


Fig. 3 Results from numerical modeling (black curves) of the experimental data (open circles) for a thin-source experiment for (top) Ar in a rhyolitic melt (Behrens and Zhang 2001) and (bottom) Th in a diopside melt (Van Orman et al. 1998). The diffusion coefficients for Ar and Th are: $D_{\text{Ar}} = 2.14 \times 10^{-8} \text{ cm}^2 \text{ s}^{-1}$ and $D_{\text{Th}} = 5.3 \times 10^{-17} \text{ cm}^2 \text{ s}^{-1}$. Note that those values are for isothermal conditions

where D_A , D_B and M_A , M_B are the diffusion coefficients and the masses of isotopes A and B, respectively, and $\gamma = 0.5$ for gases. The diffusion data are summarized in Table 1. Note that the diffusion coefficients are for material that does not match the pumice

Table 1 Arrhenius parameters used in the numerical modeling shown in Fig. 4

	E_a (kJ mol ⁻¹)	D_0 (cm ² s ⁻¹)	
Model <i>a</i>			
Ar	152.5	0.0204	Drapper and Carroll (1995)
³⁶ Ar	152.5	0.0215	Graham's law
⁸⁴ Kr	61.12	7.08×10^{-8}	Matsuda et al. (1989)
Model <i>b</i>			
Ar	152.5	0.0204	Drapper and Carroll (1995)
³⁶ Ar	152.5	0.0215	Graham's law
⁸⁴ Kr (100%)	100.5	5.84×10^{-6}	Matsuda et al. (1989)

composition because of a lack of experimental data in the literature. The results (i.e., eruption timescale) may therefore be underestimated. Moreover, Matsuda et al. (1989) indicated that their sample's shape may be affected by partial melting at 1273 K during diffusion experiments, resulting in an error of 100% on the ⁸⁴Kr diffusion coefficient. Two different simulations have been performed to take into account this variability (models *a* and *b*, see Table 1). For the simulation, we have assumed a glass wall thickness of 1×10^{-4} cm [the lower limit in pumices (Whitman and Sparks 1986)] and an exponential cooling rate, ν at 5 K s⁻¹. In our model, the initial noble gas ratios are unknown. However, it seems that an atmospheric composition could represent the starting point for most cases (Ruzié and Moreira 2010). Assuming this set of parameters, the best fit for the noble gases' isotopic and elementary ratios from our simulation was given by an eruption time of 500 s (for the model with 100% error on the ⁸⁴Kr), see Fig. 4.

However, this result needs to be used with caution. The eruption time of 500 s represents only the value for the analyzed pumices themselves, and may not be representative of the entire eruption. Moreover, the diffusion coefficients are not representative of the measured pumice composition, which may lead to underestimating the eruption time. Note, also, that only parts of the data fit the model prediction line (Fig. 4). This can be explained by the fact that the pumices were crushed to free the noble gases contained in the bubble (see Ruzié and Moreira 2010). This experimental method gives an average concentration of the noble gases over all bubbles contained within the pumice. Thus, the approximation for a constant glass wall thickness may not be applicable to the entire range of pumices analyzed. A more reliable approach would be to use noble gas concentrations for a single bubble (by drilling with an excimer laser through the pumice glass, for example). Unfortunately, such data for bubble-bearing pumice are not yet available in the literature.

Nevertheless, based on some approximations, the model seems to be able to explain the kinetic fractionation observed in some bubble-bearing pumices and also provides an eruption timescale of 500 s.

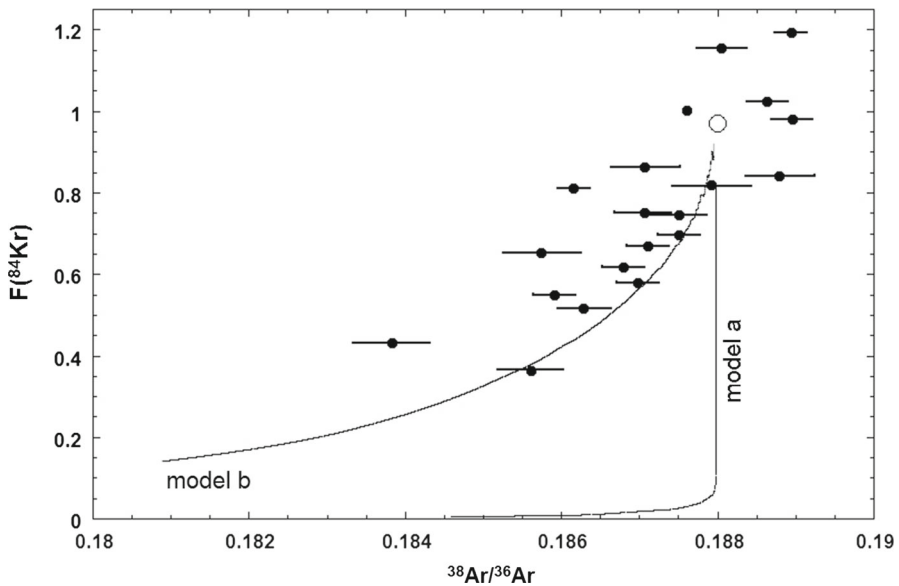


Fig. 4 Comparison between the simulation result (solid line) for model a and model b (see Table 1) and ^{84}Kr fractionation factor, $F(^{84}\text{Kr})$, versus $^{38}\text{Ar}/^{36}\text{Ar}$. $F(^{84}\text{Kr})$ represents the $(^{84}\text{Kr}/^{36}\text{Ar})_{\text{bubble}}/^{84}\text{Kr}/^{36}\text{Ar}_{\text{atmo}}$ ratio, where subscripts bubble and atmo represent the concentration in the bubble and in the air, respectively. Small solid circles are the values given by Ruzi c and Moreira (2010) for different pumices. The large unfilled circle is the atmospheric composition

6 Conclusion

This study provides a simple but rigorous mathematical approach for solving time-dependent diffusion equations with exponential temperature decay. The numerical model’s accuracy was validated with an experimental database for experiments at constant D (Van Orman et al. 1998; Behrens and Zhang 2001).

The model correctly explains some of the kinetic fractionation observed in bubble-bearing pumices by atmospheric noble gas contamination during the cooling of magma. The proposed model provides an eruption timescale if the diffusion coefficients are known and the noble gas concentrations in the bubble can be individually measured. In addition, our numerical model can be applied in studies where the variation of the diffusion equation as a function of temperature is needed.

Acknowledgements This work benefited from financial support of the Agence Nationale de la Recherche (DEGAZMAG project, contract no. ANR 2011 Blanc SIMI 5-6 003) and R gion Lorraine. This is a CRPG contribution.

References

- Amalberti J, Burnard P, Laporte D, Tissandier L, Neuville DR (2016) Diffusion of noble gases (He, Ne, Ar) in silicate glasses close to the glass transition: distinct diffusion mechanisms. *GCA* 172:107–126
- Anderson AT (1975) Some basaltic and andesitic gases. *Rev Geophys Space Phys* 13:37–55

- Behrens H, Zhang Y (2001) Ar diffusion in hydrous silicic melts: implications for volatile diffusion mechanisms and fractionation. *EPSL* 192:363–376
- Carroll MR, Stolper EM (1991) Argon solubility and diffusion in silica glass: implications for the solution behavior of molecular gases. *Geochim Cosmochim Acta* 55(1):211–225
- Crank J (1975) *The mathematics of diffusion*, 2nd edn. Clarendon Press, Oxford, p 413
- Dodson MH (1973) Closure temperature in cooling geochronological and petrological systems. *Contrib Miner Petrol* 40(3):259–274
- Drapper DS, Carroll MR (1995) Argon diffusion and solubility in silicic glasses exposed to an Ar–He gas mixture. *EPSL* 132:15–24
- Gonnermann HM, Mukhopadhyay S (2007) Non-equilibrium degassing and a primordial source for helium in ocean–island volcanism. *Nature* 449:1037–1040
- Jaupart C (2000) Magma ascent at shallow levels. In: Sigurdsson H, Houghton B, McNutt S, Rymer H, Stix J (eds) *Encyclopedia of volcanoes*. Academic Press, pp 237–245
- Kaneoka I (1980) Rare gas isotopes and mass fractionation: an indicator of gas transport into or from a magma. *Earth Planet Sci Lett* 48:284–292
- Matsuda J, Matsubara K, Yajima H, Yamamoto K (1989) Anomalous Ne enrichment in obsidians and darwin glass: diffusion of noble gas in silica-rich glasses. *GCA* 53:3025–3033
- Paonita A, Martelli M (2007) A new view of the He–Ar–CO₂ degassing at mid-ocean ridges: homogeneous composition of magmas from the upper mantle. *GCA* 71:1747–1763
- Pinti D, Wada N, Matsuda J (1999) Neon excess in pumice: volcanological implications. *J Volcanol Geotherm Res* 88:279–289
- Press WH, Teukolsky SA, Vetterling WT, Flannery BP (2007) *Numerical recipes: the art of scientific computing*, 3rd edn. Cambridge University Press, New York
- Proussevitch A, Sahagian D (2005) Bubbledrive-1: a numerical model of volcanic eruption mechanisms driven by disequilibrium magma degassing. *J Volcanol Geoth Res* 143(1):89–111
- Ruzié L, Moreira M (2010) Magma degassing process during Plinian eruptions. *J Volcanol Geotherm Res* 192:142–150
- Sparks RS (2003) Dynamics of magma degassing. *Volcan Degassing* 213:5–22
- Sparks RS, Wilson J, Hulme G (1978) Theoretical modeling of the generation, movement, and emplacement of pyroclastic flows by column collapse. *J Geophys Res* 83:1727–1739
- Tait S, Jaupart C, Vergnolle S (1989) Pressure, gas content and eruption periodicity of a shallow, crystallising magma chamber. *EPSL* 92:107–123
- Toramaru A (1995) Numerical study of nucleation and growth of bubbles in viscous magmas. *J Geophys Res* 100:1913–1931
- Van Orman JA, Grove TL, Shimizu N (1998) Uranium and thorium diffusion in diopside. *EPSL* 160:505–519
- Whitman AG, Sparks RSJ (1986) Pumice. *Bull Volcanol* 48:209–233
- Zhang Y, Cherniak DJ (2010) Diffusion in minerals and melts. *Rev Mineral Geochem* 72:p103